\$ SUPER

Contents lists available at ScienceDirect

Ecological Informatics

journal homepage: www.elsevier.com/locate/ecolinf



Assessing the distribution of nocturnal chlorophyll-a in the Northwest Pacific Ocean using ocean color and fishery echosounder acoustic data

Chuanyang Huang ^{a,b}, Yang Liu ^{a,b,*}, Jianchao Li ^{a,b,c,*}, Hailing Wang ^{a,b}, Yanping Luo ^{a,b}, Honghai Zhang ^d, Zhaohui Chen ^{c,e}

- ^a Deep Sea and Polar Fisheries Research Centre, Ocean University of China, Qingdao, China
- ^b College of Fisheries, Ocean University of China, Qingdao, China
- ^c Frontiers Science Center for Deep Ocean Multispheres and Earth System (FDOMES), Ocean University of China, Qingdao, China
- ^d College of Chemistry and Chemical Engineering, Ocean University of China, Qingdao, China
- e Key Laboratory of Physical Oceanography, Ocean University of China, Qingdao, China

ARTICLE INFO

Keywords: Nocturnal Chl-a Fishery acoustic Remote sensing Phytoplankton size class algorithm Inversion model Northwest Pacific

ABSTRACT

Phytoplankton plays a crucial role in material cycling and energy flow within marine ecosystems. Ocean color remote-sensing chlorophyll-a (Chl-a) data serves as the primary means for assessing phytoplankton in the ocean environment. Nevertheless, the determination of nocturnal Chl-a still relies heavily on in situ ocean surveys. Diel variations in Chl-a, particularly nocturnal Chl-a, can more accurately reflect the ecological processes of marine ecosystems. We aimed to probe the nocturnal Chl-a distribution in the Northwestern Pacific Ocean by examining the predator-prey dynamics (reflected by acoustic data) and phytoplankton (reflected by Chl-a data). Drawing on continuous acoustic data and observed data variation, we reprocessed the 200 kHz frequency band data. Furthermore, we derived the nocturnal Chl-a in the Northwest Pacific Ocean based on diel 200 kHz frequency band data and Phytoplankton Size Class (PSC) algorithm. The inversion model can effectively retrieve nocturnal Chl-a data, and the validation results demonstrate superior performance compared to remote sensing Chl-a data. Moreover, we discovered a robust correlation between the diurnal and nocturnal Chl-a data ($R^2 = 0.9988$, bias = 0.9925, MAE = 1.0196), indicating the feasibility of directly deriving nocturnal Chl-a data from diurnal Chl-a. This study innovatively integrates the characteristics of acoustic data for day-night monitoring and satellite remote sensing for large-scale monitoring, enabling large-scale observations of nocturnal Chl-a. The results deepen our understanding of diel ecological changes in the Northwest Pacific Ocean, provide a foundation for studying marine productivity variations and carbon cycling processes in the area, and contribute to the improvement of the monitoring and management of fishery activities in the region.

1. Introduction

Phytoplankton underpin marine ecosystem productivity through biogeochemical cycling, and their community composition and quantity directly mediate carbon export efficiency and trophic energy transfer. As primary producers in the ocean, phytoplankton absorb carbon dioxide through photosynthesis, produce organic matter, and release oxygen, forming the foundation of the marine food chain (Falkowski et al., 2004; Field et al., 1998; Hilligsøe et al., 2011). The organic matter produced is transferred to zooplankton and subsequently to fish and other marine organisms, facilitating energy exchange within marine ecosystems (Ariza et al., 2015; Everett et al., 2017).

The Northwest Pacific Ocean is one of the world's most productive regions. According to the Food and Agriculture Organization (FAO) of the United Nations, fishery production in the Northwest Pacific reaches 20 million tons, accounting for 25 % of global marine fish production (FAO, 2019). Ocean currents and mesoscale eddies form fronts in this area, particularly in the Kuroshio Extension, providing nutrient-rich water (Wang et al., 2021; Zhou et al., 2021). Monitoring and analyzing plankton, especially phytoplankton, improves understanding of marine environmental changes driven by climate change and supports marine ecosystems and fishery resource protection (Friedland et al., 2012; Hays et al., 2005; Yatsu et al., 2013).

Remote sensing of chlorophyll-a (Chl-a) data has been extensively

^{*} Corresponding authors at: Deep Sea and Polar Fisheries Research Centre, Ocean University of China, Qingdao, China. *E-mail addresses*: yangliu315@ouc.edu.cn (Y. Liu), lijianchao@ouc.edu.cn (J. Li).

utilised to study phytoplankton and fisheries in the Northwest Pacific region (Chai et al., 2021; Fan et al., 2009; Tian et al., 2022). Acoustic methods can also be applied in plankton investigations. Although directly detecting phytoplankton remains challenging, larger zooplankton can be detected and combined with sampling to study plankton biodiversity and distribution characteristics (Chiba et al., 2013; Zang et al., 2023). Both phytoplankton and zooplankton exhibit distinct diel differences (Garcia-Herrera et al., 2022; Guan et al., 2023). However, only a few studies have integrated multiple data sources to examine these differences, especially nocturnally. Additionally, numerous fishery activities in the Northwest Pacific Ocean occur at night due to the diel vertical migration (DVM) of prey species. Thus, relying solely on marine surveys or remote sensing data collected during the daytime may provide a limited or biased perspective, particularly when predicting fishing ground distribution. Collecting data at night and integrating multiple data sources could substantially enhance research in this field.

With the development of remote sensing technology, phytoplankton observations can be indirectly obtained using Chl-a data from ocean color remote sensing (Boyce et al., 2010; Dutkiewicz et al., 2019). The Phytoplankton Size Class (PSC) Algorithm (Brewin et al., 2010; Huan et al., 2022) classifies phytoplankton into picophytoplankton (<2 µm, Pico), nanophytoplankton (2-20 µm, Nano), and microphytoplankton (>20 μm, Micro) using diagnostic pigment analysis (DPA) of in-situ pigment data measured by high-performance liquid chromatography (HPLC) (Uitz et al., 2006). This algorithm has been widely applied in studies on the strong relationship between size and phytoplankton function (Brewin et al., 2011; Turner et al., 2021; Xi et al., 2020). Because ocean color remote sensing relies on sunlight, observations are limited to daytime. However, continuous station monitoring studies have revealed significant diel variations in Chl-a concentration, community composition, and Chl-a fluorescence (Doblin et al., 2011; Guan et al., 2023; Neveux et al., 2003; Pan et al., 2019). Despite known diurnal differences in Chl-a characteristics, comprehensive large-scale observations of nocturnal Chl-a remain lacking.

Acoustic methods are valuable for underwater biological detection, fishery resource assessment, and management (Carlsen et al., 2024; Sánchez-Gendriz and Padovese, 2017; Zhu et al., 2024). They offer high spatiotemporal resolution, large measurement ranges, and minimal environmental disturbance (Béhagle et al., 2016; Xue et al., 2021). Relevant acoustic equipment includes the Acoustic Doppler Current Profiler (ADCP) and echosounders. Among these, multi-frequency echosounders have greater particle-detection capability, enabling simultaneous detection at close range, whereas low-frequency beams detect large organisms at greater distances (Holliday, 1995). Because the acoustic equipment relies on sound waves, it is unaffected by day-night cycles. Consequently, acoustic devices are commonly used for continuous station and transect observations, and can be combined with remote sensing data to investigate subsurface and diel variations in the ocean, such as zooplankton vertical migration or marine environmental profiling (Behrenfeld et al., 2019; Schwartz-Belkin and Portman, 2023). While acoustic devices can be integrated with other data for ecological investigations (Agarwal et al., 2016; Fujioka et al., 2014; Kande et al., 2024), few studies have explored their integration with remote sensing and algorithms for enhanced data analysis (Behrenfeld et al., 2019).

Although acoustic data cannot directly detect phytoplankton, they effectively monitor plankton (Béhagle et al., 2016; Holliday, 1995; Lavery et al., 2007). The association between plankton DVM and phytoplankton provides a basis for linking phytoplankton to acoustic data (Fernández-Álamo and Färber-Lorda, 2006). Specifically, acoustic data is capable of capturing signals from zooplankton that undergo DVM to surface layers for feeding activities (Behrenfeld et al., 2019). These zooplankton-mediated vertical movements subsequently induce quantitative changes in phytoplankton populations through trophic interactions (Fogg, 1991; Zhou et al., 2015). Consequently, the observed diel variations in acoustic signals exhibit a strong correlation with

phytoplankton dynamics, establishing an indirect but functionally significant linkage between acoustic signatures and phytoplankton abundance. We used Chl-a as a proxy for phytoplankton. By leveraging the complementary strengths of remote sensing and multi-frequency acoustic data, we first mapped nocturnal Chl-a distribution. Specifically, we established relationships between nocturnal Chl-a data and acoustic data, as well as between diurnal remote sensing Chl-a data and acoustic data. This enables the estimation of nocturnal Chl-a using daytime remote-sensing Chl-a data. The PSC algorithm bridges acoustic detection of planktonic particles and Chl-a data, ultimately allowing nocturnal Chl-a estimation in the Northwest Pacific Ocean from diurnal ocean color data.

2. Materials and methods

2.1. Study area and data collection

The study area is situated in the Northwest Pacific Ocean, extending from 140°E to 170°E and 30°N to 50°N . Fig. 1 depicts the range covering all sampling stations.

2.1.1. In situ data collection and remote sensing data

Fishery echosounder acoustic data and surface Chl-a (Chl-a $_{sur}$) data at a depth of 3.5 m were collected during a research cruise in November 2019 aboard the research vessel "Dongfanghong 3". Data were collected continuously along the longitudinal section at 150°E. Chl-a $_{sur}$ data was collected by Turner Designs Cyclops-7 fluorescence sensor. Furthermore, in-situ Chl-a $_{in}$ situ) was sampled at a depth of 5 m.

Echosounder data were acquired using a Simrad EK80 echosounder system with five transducers operating at 18, 38, 120, 200, and 333 kHz frequencies. The system was calibrated using the standard sphere method (Foote et al., 1987), transmitting pulses in sequence for 1.024 ms in FM mode. Chl-asur data were obtained using a surface water sampling system. Remote-sensing Chl-a data (Chl-amodis) were sourced from the NASA Ocean Color Website (MODIS-Aqua) with a monthly temporal and spatial resolution of 4 km. Chl-amodis data primarily represent daytime conditions, while nocturnal Chl-a data are sourced from Chl-asur collected during the cruise.

2.2. Data processing

2.2.1. Chl-a data processing

Given the study's objective of retrieving nocturnal Chl-a concentrations through satellite-derived Chl-a data, where satellite data serve as the foundational dataset, our analytical framework necessitates maintaining consistency in concentration scales between Chl-a $_{\rm sur}$ and Chl-a $_{\rm modis}$. To address inherent disparities in measurement protocols, we implemented a linear regression-based normalization of Chl-a $_{\rm sur}$ data against match-up Chl-a $_{\rm modis}$. Chl-a $_{\rm sur}$ data were then separated into daytime and nighttime datasets. Chl-a $_{\rm modis}$ data were extracted based on the sampling locations of the acoustic data.

Phytoplankton size components were determined using the PSC algorithm, which classifies phytoplankton into picophytoplankton (0.2–2 $\mu m,\ C_1),\ nanophytoplankton\ (2–20 <math display="inline">\mu m,\ C_2),\ and\ microphytoplankton\ (>20 <math display="inline">\mu m,\ C_3).$ The algorithm separates Chl-a into C_3 and $C_{1,2}$, where $C_{1,2}$ is the sum of C_1 and C_2 . $C_{1,2}$ was further divided into C_1 and C_2 using the following equations:

$$C_{1,2} = C_{1,2}^m \bullet [1 - \exp(-S_{1,2} \bullet C)], \tag{1}$$

$$C_1 = C_1^m \bullet [1 - \exp(-S_1 \bullet C)], \tag{2}$$

$$C_2 = C_{1,2} - C_1, (3)$$

$$C_3 = C - C_{1,2} \tag{4}$$

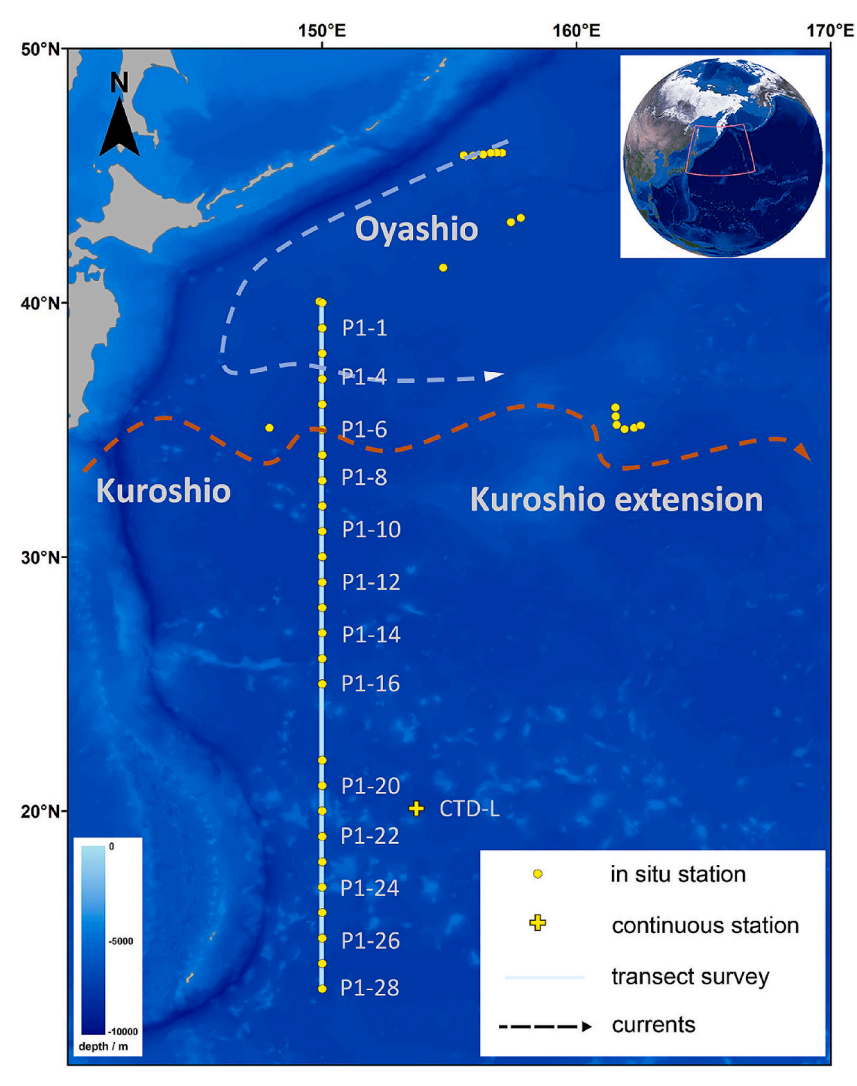


Fig. 1. The sampling station and survey route in the Northwest Pacific Ocean.

where $C_{1,2}^m$ and C_1^m determine the upper limit values of $C_{1,2}$ and C_1 . $S_{1,2}$ and S_1 determine the increase in the two phytoplankton size components with Chl-a concentration (Table 1).

2.2.2. The correction and reprocessing of fishery echosounder acoustic data

The 200 kHz and 333 kHz echosounder data were processed using Echoview software to eliminate background noise, invalid pings, and spike noise. The data were then integrated over 2 m depth bins and 10-min intervals to calculate backscattering values (Sv, dB re m⁻¹), which were then averaged over time. To ensure consistent diurnal and nocturnal categorization while minimizing the influence of latitude on photoperiod length, we defined fixed time intervals. Specifically, day-time was set from 08:00 to 16:00 local time, and nighttime spanned from 20:00 to 04:00. This approach effectively circumvents the issue of variable day and night lengths that typically occur with changes in latitude. To minimize vessel noise interference, the top 20 m of the water column was excluded, and data were averaged over the 20–30 m depth range to capture plankton diel vertical migration signals in the study area. This

Table 1The coefficients of PSC algorithms.

Coefficients	$C_{1,2}^m/C_1^m$	$S_{1,2}/S_1$
Nano- and picophytoplankton	1.057	0.851
Picophytoplankton	0.107	6.801

approach aligns with previous studies, which have shown that this layer of the water column predominantly contains plankton patches information (Swartzman et al., 1999; Tokarev et al., 1998).

High-frequency fishery echosounder bands can be used to detect smaller particles in the water column. Additionally, the different frequency bands of the fishery echosounder exhibit disparities in the Sv data received from the same objects detected in the water. The Sv data of the particles detected from the lower-frequency band tend to be stronger than those from the higher-frequency band. Therefore, variations in Sv data differed across frequency bands. In this study, nocturnal Sv data were used to reprocess diurnal 200 kHz data. The data were divided using 26°N as the boundary. South of 26°N, daytime 333 kHz Sv predominantly reflects smaller, non-migratory particles, enabling clearer isolation of nocturnal migrant backscatter. However north of 26°N, larger-bodied zooplankton persisting in surface waters during daytime disproportionately contribute to Sv signals at elevated latitudes, masking the DVM-specific backscattering values. Therefore, we implement detection characteristics of different acoustic frequency bands to eliminate zooplankton latitudinal size-spectra effects. The reprocessing algorithms are as follow:

$$(Sv333'_d + I) - (Sv200'_d + \delta I) = \Delta_{Sv333d - Sv200d}$$
(5)

$$Sv200_{d_re} = Sv200_d + I$$
 (6)

where $Sv333_d'$ and $Sv200_d'$ represent the average daytime data at 333 kHz and 200 kHz south of 26°N. The variable I is the influence coefficient, representing the impact of plankton particles detected by the 333 kHz frequency band. The constant δ , valued at 3.042, is derived from the average ratio of diurnal to nocturnal Sv data for the two frequency bands south of 26°N. Nocturnal data from this region serve as a reference for the influence of larger plankton particles on Sv data. $\Delta_{Sv333d-Sv200d}$ denotes the difference in diurnal Sv data for the two frequency bands north of 26°N before correction, while $Sv200_{d-re}$ represents the corrected diurnal Sv data at 200 kHz north of 26°N.

2.2.3. Nocturnal Chl-a algorithm construction

In this study, a hyperbolic model was adopted to establish the relationship between the different components of Chl-a and Sv data. The independent variables were Chl-a concentration and its components. The algorithm is as follows:

$$\Delta_{Sv} = \frac{\mathbf{a} \bullet \mathbf{C}}{(b+C)} \tag{7}$$

where Δ_{SV} denotes the difference in Sv data,C denotes Chl-a or different phytoplankton size components, and a and b are the algorithm coefficients. This model depicts the trend of the Sv data as the Chl-a concentration or the concentration of different phytoplankton size components changes.

During the collection of Sv data along $150^{\circ}E$ longitude, simultaneous day-night Sv data were available at a single location. Therefore, we averaged the 200 kHz Sv data over a day-night period. We selected the midpoint of the latitude range traversed within that day-night period as the corresponding latitude and longitude position for that period's Sv data. The data were further used to construct the relationship between the Sv data and latitude variation. In the subsequent relationship modelling, the corresponding Sv data were obtained based on latitude. According to Eq. (7), the difference between the nocturnal 200 kHz Sv data and the corrected diurnal 200 kHz Sv data is related to C_3 as follows:

$$\Delta_{\text{SY200n-Sv200d-re}} = \frac{\mathbf{a} \bullet C_3}{(b + C_3)} \tag{8}$$

Diurnal C_3 was calculated by applying the PSC algorithms to Chla a_{modis} , and nocturnal C_3 was derived from Chl- a_{sur} . Diurnal and nocturnal C_3 data were connected using $\Delta_{Sy200n-Sy200d-re}$, and the distribution of nocturnal Chl-a was obtained based on the relationship between C_3 and Chl-a.

2.2.4. Algorithm assessment and validation

The corresponding nocturnal Chl-a data were extracted for validation based on the position of Chl-a $_{\rm in\ situ}$. The slope, intercept, and R² values between Chl-a $_{\rm in\ situ}$ and nocturnal Chl-a data were recorded to assess algorithm performance. Additionally, the bias and mean absolute error (MAE) were calculated to quantify the systematic bias of the algorithm (the closer the bias value was to 1, the lower the deviation; a bias of 1 indicated no deviation) (Seegers et al., 2018). These results were then compared with those obtained for Chl-a $_{modis}$. Fig. 2 illustrates the research process used in this study.

$$Bias = 10^{\sum_{i=1}^{n} \left(log_{10}\left(chl_{nighttime}\right) - log_{10}\left(chl_{in \, situ}\right)}{n}\right)}$$
 (9)

3. Results

3.1. Diel variation of Chl-a and Sv data

3.1.1. Chl-a data

Chl- a_{sur} was differentiated between the day and night, and diurnal Chl- a_{sur} was compared with Chl- a_{modis} (Fig. 3). As shown in Fig. 3, although the results indicate an apparent overestimation of the Chl- a_{sur} data, the overall relationship followed a linear pattern, as indicated by the R^2 value. To ensure consistency, the Chl- a_{sur} data were corrected based on regression results so that the measurement results of Chl- a_{sur} and Chl- a_{modis} were on the same observational scale.

The diel variation of the corrected Chl- a_{sur} is shown in Fig. 4, where red dots represent diurnal Chl- a_{sur} data, blue dots represent nocturnal Chl- a_{sur} data, and gray dots represent Chl- a_{sur} data outside the selected daytime and nighttime periods, consistent with the Sv data. Chl- a_{sur}

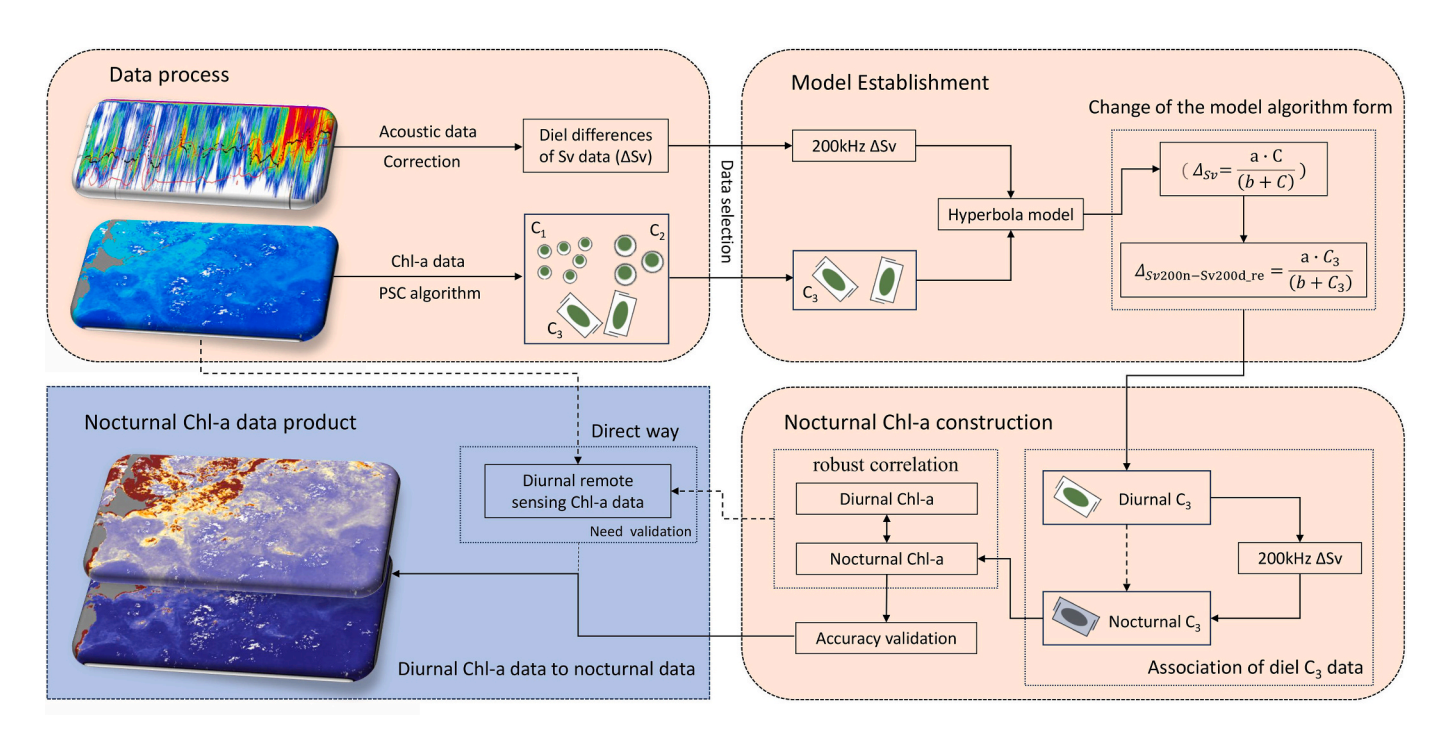


Fig. 2. The flowchart of nocturnal Chl-a acquisition.

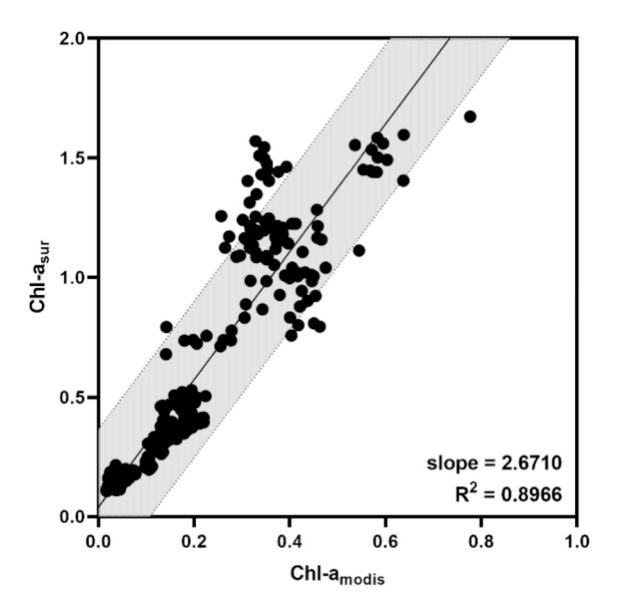


Fig. 3. The fitting result between the initial Chl- $a_{\rm sur}$ and Chl- $a_{\rm modis}$. The two dashed lines represent the 95 % confidence interval, and the solid line indicates the regression line.

exhibited significant diel fluctuations: during the day, the Chl-a_{sur} concentration initially decreased before increasing, while at night, it first increased and then decreased. Furthermore, the overall Chl-a_{sur} concentration during the nighttime was higher than during the daytime, with a mean diel difference of 0.12 mg m $^{-3}$ in the study area. The corrected Chl-a_{sur} values were subsequently divided into phytoplankton concentrations using the PSC algorithm.

To further validate these results, we selected data from a continuous monitoring station outside the study area (20.1°N, 153.7°E) for analysis. The diel variation trend of Chl-a data from the CTD measurements (collected by Sea-bird WET Labs ECO-FLNTUrtd fluorescence sensor in the depth of 3.5 m) closely aligned with that of Chl-a $_{sur}$ in the study area (Fig. 5).

3.1.2. Sv data

To better distinguish the differences between daytime and nighttime data and illustrate diel variations, we designated local time 8:00–16:00 as diurnal data and 20:00–4:00 (following day) as nocturnal data. Fig. 6 illustrates the data variations during the survey along $10^\circ N$ to $40^\circ N$ and $150^\circ E$. In the upper part of Fig. 6, the red dots represent diurnal 200 kHz Sv data, blue dots represent nocturnal Sv data, and gray dots represent Sv data outside the selected daytime and nighttime periods. The results

indicate that during continuous diel changes, the intensity of Sv data was lower during the day than at night.

The lower part of Fig. 6 shows the trend of Chl-a_{sur} with increasing latitude. At lower latitudes, primarily influenced by the Kuroshio Current, Chl-a concentration remained low with daytime concentrations lower than nighttime concentrations. North of 35° N, the region gradually came under the influence of the Oyashio Current, leading to an increase in Chl-a concentration (as shown in Fig. 4). Notably, the diel variations in 200 kHz Sv data and Chl-a concentration exhibit distinct trends with latitude. While Sv data showed a gradual increase with latitude, Chl-a concentration exhibited a obvious rise under the Oyashio Current's influence

Further analysis of 333 kHz and 200 kHz Sv data revealed that at lower latitudes, there existed a difference in Sv intensity between the two frequency bands, with 333 kHz Sv values notably higher than those at 200 kHz. However, as latitude gradually increased, the difference between Sv intensities at the two frequencies diminished (Fig. 7). This phenomenon can be attributed to the detection characteristics of the echosounder. In low-latitude regions, smaller suspended particles dominate the water column, which are detected more effectively by the higher-frequency 333 kHz band. As latitude increases, particle size also increases, allowing the 200 kHz band to detect larger suspended particles more efficiently. Moreover, due to the differing Sv characteristics of

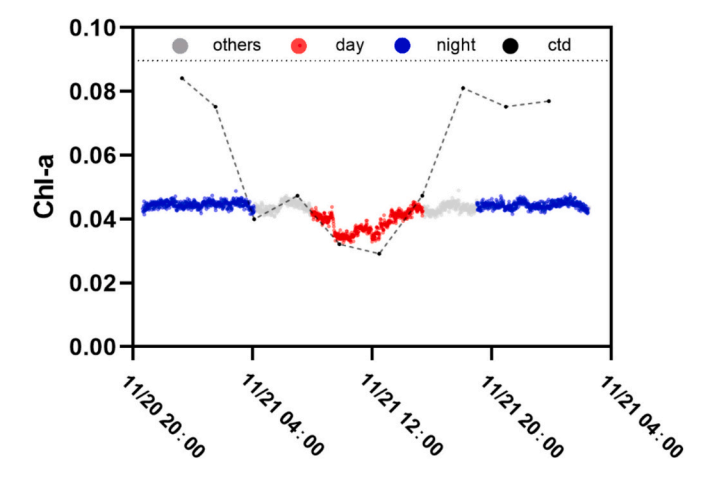


Fig. 5. The diel variation of the corrected Chl-a $_{sur}$ in a continuous station. Red dots represent diurnal Chl-asur data, blue dots represent nocturnal Chl-asur data, gray dots represent Chl-asur data outside the selected daytime and nighttime periods, and black dots represent Chl-a collected using CTD. (For interpretation of the references to color in this figure legend, the reader is referred to the web version of this article.)

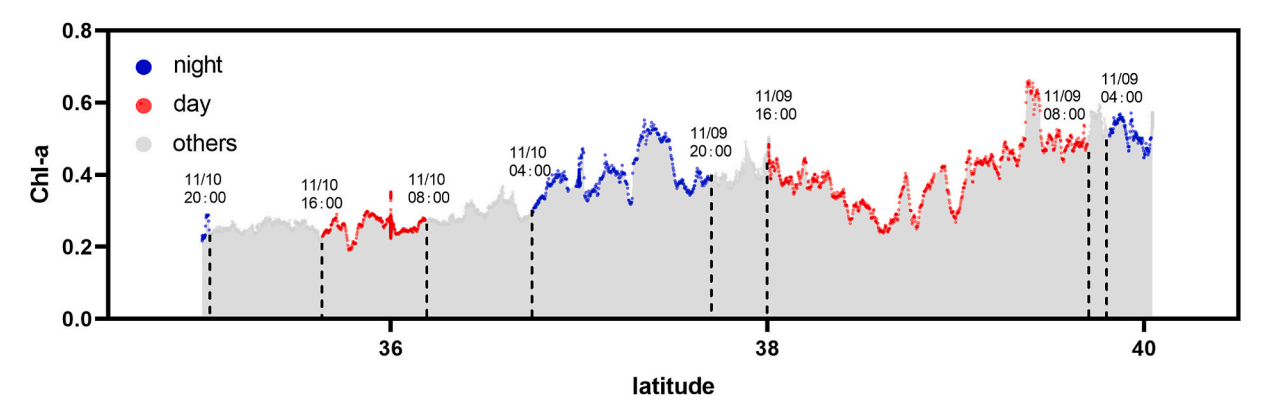


Fig. 4. The diel variation of the corrected Chl-a_{sur}. Red dots represent diurnal Chl-a_{sur} data, blue dots represent nocturnal Chl-a_{sur} data, and gray dots represent Chl-a_{sur} data outside the selected daytime and nighttime periods. (For interpretation of the references to color in this figure legend, the reader is referred to the web version of this article.)

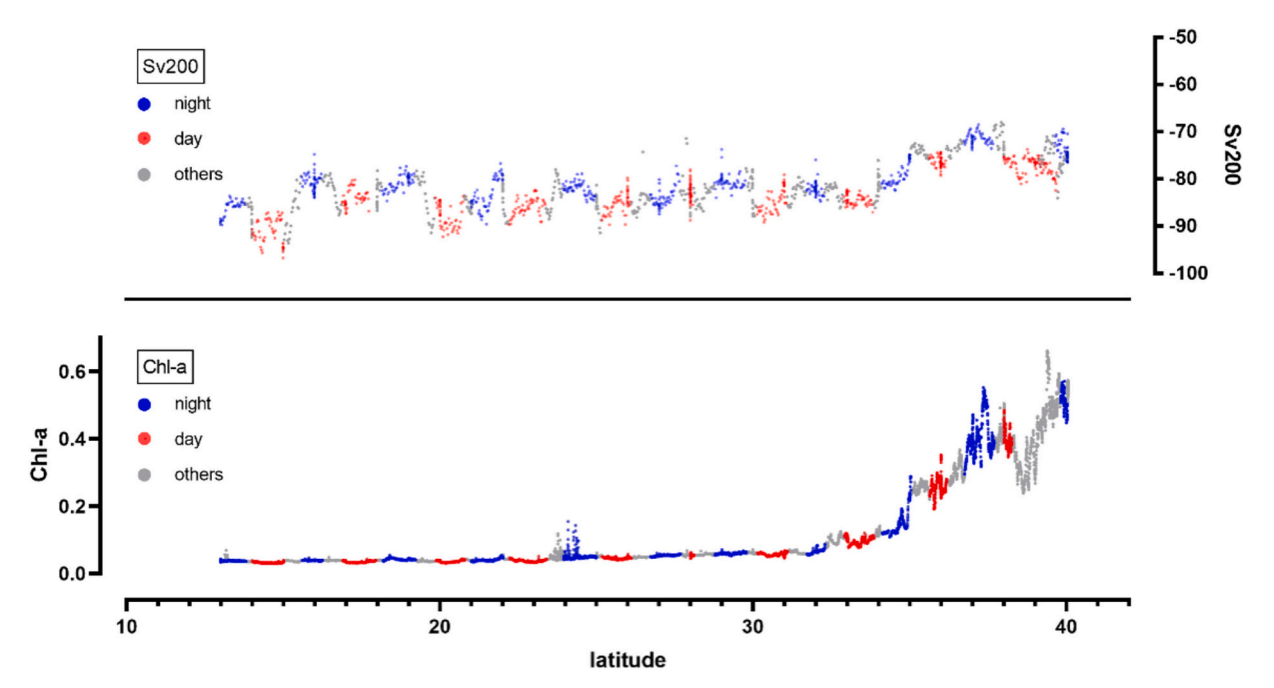


Fig. 6. The diel variation of 200 kHz Sv data and Chl-a_{sur} data during the survey. Red dots represent diurnal data, blue dots represent nocturnal data, and gray dots represent data outside the selected daytime and nighttime periods. The upper part illustrates the variation of 200 kHz Sv data, while the lower part displays Chl-a_{sur} data. (For interpretation of the references to color in this figure legend, the reader is referred to the web version of this article.)

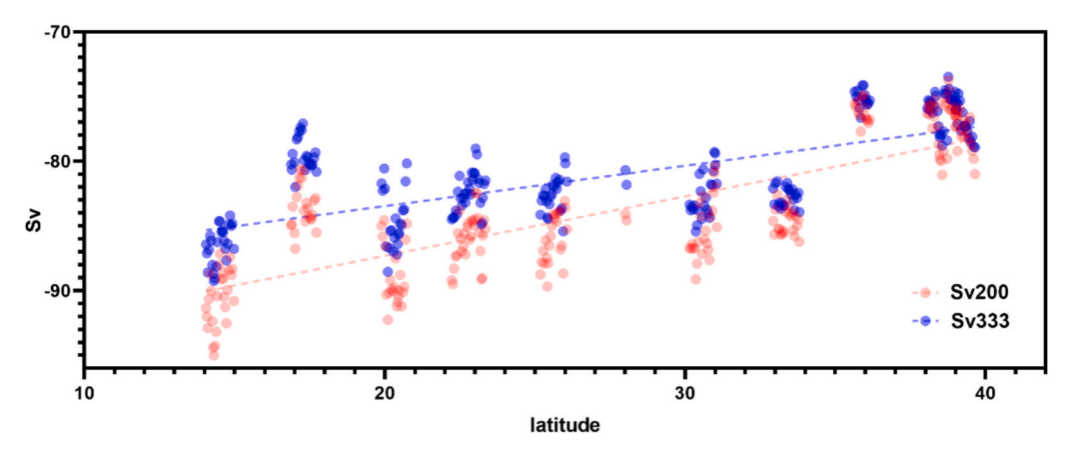


Fig. 7. The variation of 200 kHz and 333 kHz Sv data with latitude.

the echosounder at different frequency bands, the Sv intensity at 200 kHz was higher than at 333 kHz, causing the Sv data from both frequencies to gradually converge as latitude increased. Therefore, we reprocessed the diurnal 200 kHz Sv data and further examined the differences between the two frequency bands.

During the reprocess of acoustic data, $26^{\circ}N$ was chosen as the boundary, marking the approximate location of the biogeographic province at $150^{\circ}E$ (Zang et al., 2023). Sv data were not processed south of $26^{\circ}N$, as they were primarily influenced by smaller suspended particles that affect 333 kHz Sv data but are not effectively detected by the 200 kHz frequency band. Plankton abundance and size gradually increased north of $26^{\circ}N$. Fig. 8 illustrates the difference in Sv data between the two frequency bands during the daytime and nighttime, obtained by averaging Sv data over both periods and selecting the midpoint latitude of the travelled distance.

As shown in Fig. 8, south of 26° N, the difference in Sv data remained relatively stable. During nighttime, the average enhancement of the 200 kHz Sv data relative to the 333 kHz Sv data was 3.042 (δ , Eq. (5)) compared to daytime. In this study, we used the nighttime enhancement

of 200 kHz Sv data south of $26^{\circ}N$ —caused by the upward movement of zooplankton—as a reference to reprocess the diurnal 200 kHz data north of $26^{\circ}N$. This process mitigates the influence of larger suspended particles on the diurnal 200 kHz Sv data in the northern region.

Fig. 9 illustrates the difference in Sv data between the 333 kHz and 200 kHz frequency bands before and after correction. The gray dots represent the original differences, while the red dots indicate the corrected data. After correction, the increased difference between the two frequency bands reflects a higher abundance of smaller suspended particles with increasing latitude.

To further investigate diel variation, we analysed the relationship between 200 kHz Sv data (including both nocturnal and corrected diurnal data) and latitude (Fig. 10). After filtering out outliers influenced by eddies and other external factors, we established a relatively stable relationship between diel variation in 200 kHz Sv data and latitude. This relationship allows for the estimation of diel differences in 200 kHz Sv data at corresponding latitudes. Notably, the magnitude of diel differences increases with latitude.

C. Huang et al. Ecological Informatics 90 (2025) 103246

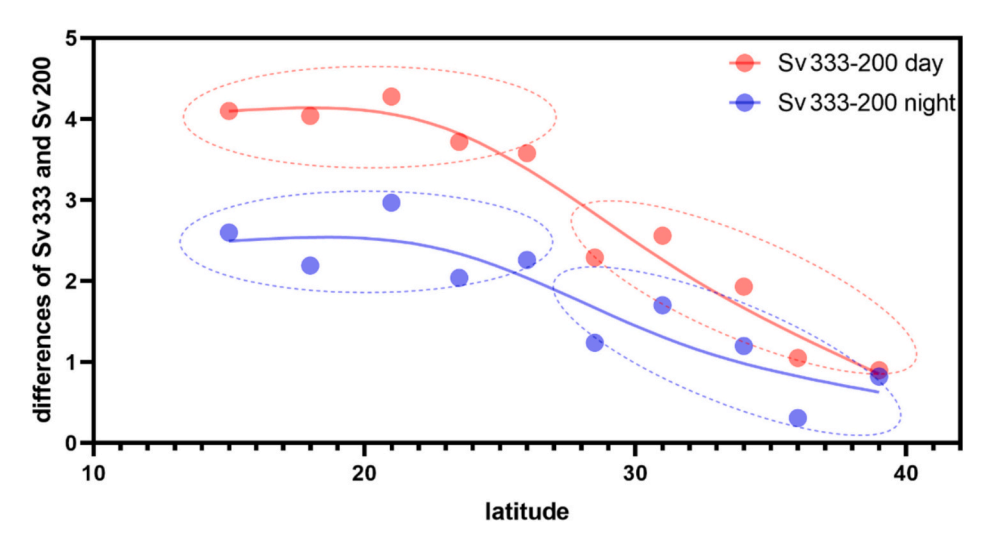


Fig. 8. The variation of the differences between two frequency bands Sv data with latitude during daytime and nighttime.

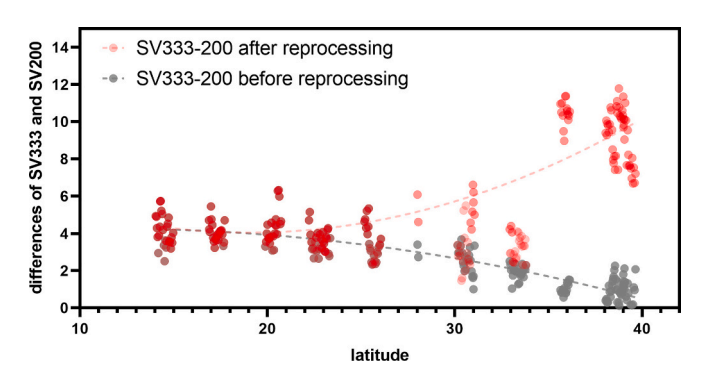


Fig. 9. Variation in the differences between diurnal Sv data at 333 kHz and 200 kHz before and after correction across latitude.

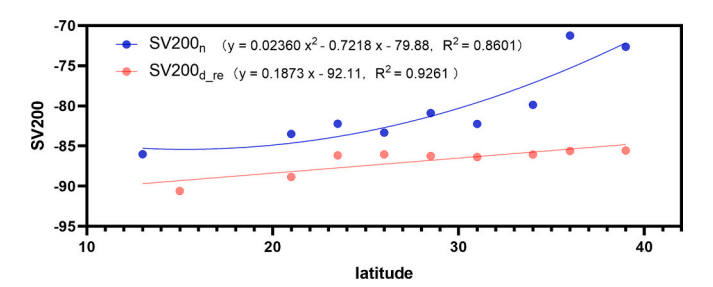


Fig. 10. The relationship between 200 kHz Sv data (nocturnal data and diurnal data after correction) and latitude.

3.2. Relationship between Chl-a data and Sv data

Fishery echosounder cannot directly detect small particles such as phytoplankton. In this study, we applied the processing method described in Section 2.2.2 to reprocess the diurnal 200 kHz Sv data, eliminating the influence of large plankton during daytime. Therefore, the diel difference in 200 kHz Sv data primarily reflects the information of zooplankton that ascend to surface water layer through DVM during nighttime. To classify Chl-a data into different phytoplankton size classes, we employed the PSC algorithm. This study established a relationship between the Sv data associated with larger particles—reflected by the diel difference in 200 kHz Sv data—and the C₃ phytoplankton component derived from the PSC algorithm.

The relationship between diurnal C₃, calculated from Chl-a_{modis}, and

the diel difference in 200 kHz data is illustrated in Fig. 11(a). This relationship follows a hyperbolic model, with an $\rm R^2$ value of 0.9182. The two dashed lines in Fig. 11(a) represent the 95 % confidence intervals. Based on this model, the diel difference in 200 kHz data can be inferred from remote sensing Chl-a data, primarily reflecting the distribution of larger particles during nighttime.

Similarly, we established a relationship between the nocturnal C_3 component, obtained from nocturnal Chl-a $_{sur}$ data via the PSC algorithm, and the diel difference in 200 kHz data using the hyperbolic model (Fig. 11(b)), yielding an R^2 of 0.9156. The dashed lines indicate the 95 % confidence intervals. By linking C_3 obtained values derived from Chl-a $_{modis}$ and Chl-a $_{sur}$ data with the diel difference in 200 kHz SV data, we created a method to connect diurnal and nocturnal Chl-a data, allowing the retrieval of nocturnal Chl-a from information from remote sensing Chl-a data.

Because the C_3 component cannot be directly obtained using the PSC algorithm, we identified a quadratic function that effectively models the relationship between Chl-a and C_3 (Fig. 12). This relationship, based on nocturnal Chl-a_{sur} and C_3 data, exhibited a strong correlation, with an R^2 value of 0.9998. The coefficients for the hyperbolic models are presented in Table 2 and can be used to derive nocturnal Chl-a data from Chl-a_{modis} (Fig. 13).

3.3. Accuracy validation of nocturnal Chl-a

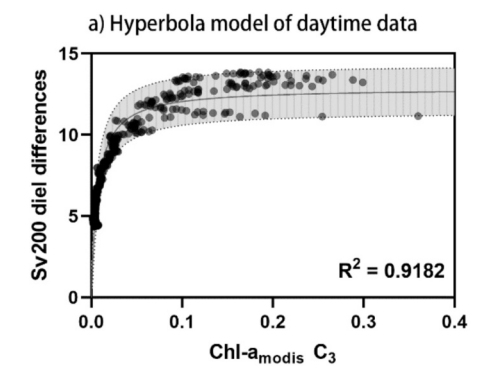
Nocturnal Chl-a data were validated against Chl- $a_{in\ situ}$, and validation was performed between Chl- a_{modis} and Chl- $a_{in\ situ}$ for comparison. The results are shown in Fig. 14. The R^2 for the validation of nocturnal Chl-a against Chl- $a_{in\ situ}$ was 0.6714, with a slope of 1.100 and an intercept of 0.0439. The validation results for Chl- a_{modis} showed an R^2 value of 0.6625 with a slope of 1.135 and an intercept of 0.0141. The systematic biases are presented in Table 3. The overall systematic bias for the nocturnal Chl-a data may be better than that for Chl- a_{modis} .

Additionally, we discovered a strong correlation between diurnal and nocturnal Chl-a, with an R^2 of 0.9988, a bias of 0.9925, and an MAE of 1.0196, enabling the estimation of nocturnal Chl-a distribution based on diurnal Chl-a (Fig. 15). Although this result requires more in situ data for validation, it provides a concise way to obtain nocturnal Chl-a data.

4. Discussion

4.1. The latitudinal trend fishery echosounder Sv data in Northwest Pacific Ocean

Previous studies have shown that the Sv of Fluid-like (FL) class,



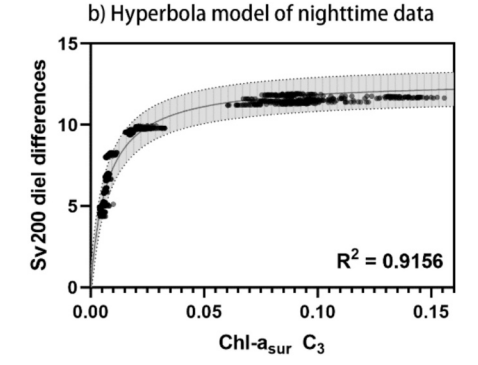


Fig. 11. a) Relationship between diurnal C_3 (Chl- a_{modis}) and diel difference in 200 kHz Sv data, modelled using a hyperbolic function. b) Relationship between nocturnal C_3 (Chl- a_{sur}) and diel difference in 200 kHz Sv data, also modelled using a hyperbolic function. The dashed lines represent the 95 % confidence interval, while the solid line represents the fitted line.

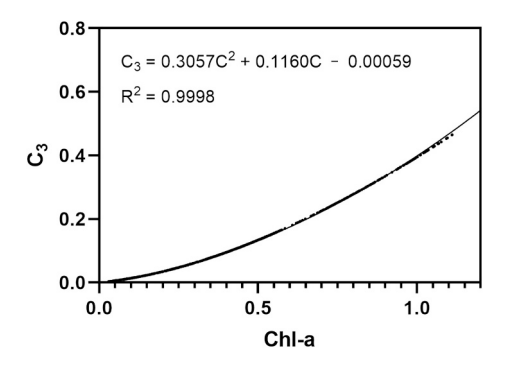


Fig. 12. Quadratic function describing the relationship between nocturnal Chla $_{\hbox{\scriptsize sur}}$ and $C_3.$

Table 2 Coefficients of the hyperbolic models describing the relationship between C_3 and the diel difference in 200 kHz Sv data.

Coefficients	a	b
Chl-a _{modis} C ₃ (daytime)	12.88	0.007250
Chl-a _{sur} C ₃ (nighttime)	12.74	0.006871

which includes copepods, euphausiids, and chaetognaths, typically increases from low- to high-frequency acoustic backscatter from 18 to 200 kHz frequency band, and plankton show a rapid rise in the scattering levels within the lower frequency range and a tendency toward levelling off at higher frequencies (Nie et al., 2023; Stanton, 2000; Ventero et al., 2020). These results are consistent with our findings. South of 26°N, the suspended particles mainly consisted of smaller organisms that could be detected at a higher frequency (333 kHz), and the 333 kHz band shows considerably higher values than the 200 kHz, which is consistent with the biogeographic provinces around 150°E (Zang et al., 2023). North of 26°N, the Sv data for the two frequency bands gradually increased and converged. This can be attributed to two main factors. First, as latitude increases, the abundance and size of planktonic organisms increase with changes in the marine environment (Zang et al., 2023). Consequently, the Sv data for both the frequency bands gradually increase. Second, owing to the larger size of the suspended particles, the 200 kHz frequency band detected higher Sv intensities from the same particles than the 333 kHz frequency band. Hence, although the 333 kHz frequency band can detect a greater number of suspended particles, the trend and intensity difference of the Sv data between the two frequency bands gradually converge (Stanton, 2000). This further demonstrates that there is a certain variation pattern of Sv data with latitude, a connection driven by latitudinal gradients in environmental controls (like temperature, salinity) and nutrient regimes, which collectively alter plankton community composition (McManus and Woodson, 2012; Messié and Chavez, 2017; Zang et al., 2023). Although Xue et al. showed no obvious correlation between Sv data and latitude—owing to the different collection times of the acoustic data—Sv data are affected by the DVM of zooplankton, and the latitude span is relatively small (Xue et al., 2021). Therefore, we averaged the data over the daytime periods. This approach can not only distinguish the day–night Sv data conditions but also explore the relationship between Sv data and latitude.

Based on the above analysis, because of the characteristics of the 333 kHz frequency band, it cannot fully reflect the situation of suspended particles at night. If we directly use the results of the day-night difference of 200 kHz data, it may lead to the omission of suspended particles that exist in the surface layer both during the day and at night north of 26°N. Therefore, in our study, we selected the daytime data of 200 kHz north of 26°N, and based on the enhancement in Sv data caused by the DVM south of 26°N, we reprocessed the enhancement of the diurnal 200 kHz frequency band caused by the increase in latitude. However, the changes caused by DVM and the variation in planktonic organisms with latitude are not entirely consistent, with differences in the intensity and species composition of plankton (Behrenfeld et al., 2019; Zang et al., 2023). Seasonal variations in planktonic organisms may also contribute to the uncertainties in the reprocessing process (Garcia-Herrera et al., 2022; Wei et al., 2023; Zhou et al., 2015). Given the limitations of the Sv data and the calibration process, we delimited the study range from 30°N to 50°N, and the relevant results of the Sv data reprocess may not be applicable to other marine regions. Further seasonal studies and validation are required. Simultaneously, different processing methods can be applied to the Sv data to leverage the multi-frequency and day-night detection advantages of the fishery echosounder, enabling further analysis of the correlation between the Sv data and latitude or the marine environment.

4.2. Potential relationships in model construction

This study investigated the relationship between suspended particles and Chl-a in the water column by establishing a connection between the diel variation of surface 200 kHz Sv data and different sizes of Chl-a components. Although the 200 kHz frequency band of the fishery echosounder does not directly detect phytoplankton, the Sv data containing zooplankton information exhibits a stable correlation (represented by hyperbolic model) with the large phytoplankton represented by the C₃ component calculated using the PSC algorithm. The PSC algorithm has been widely used and validated in previous studies for its capacity to characterize biomass relationships between plankton groups (Brewin et al., 2010; Huan et al., 2022). Therefore, we selected the hyperbolic model based on its alignment with the general trends of the PSC algorithm model and its superior statistical fitting performance.

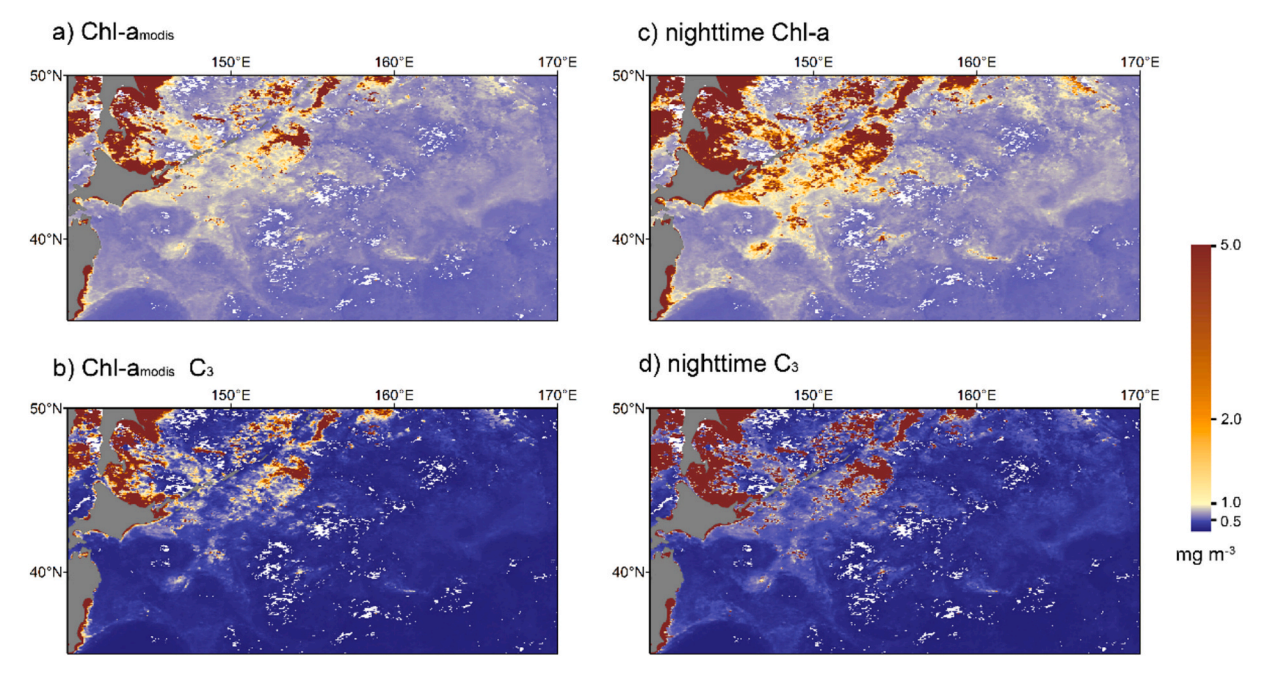


Fig. 13. Distribution of Chl-a. a) is the distribution of Chl-a $_{modis}$ from MODIS-Aqua. b) is C_3 component calculated through PSC from Chl-a $_{modis}$. c) is the nocturnal Chl-a distribution. d) is the nocturnal C_3 distribution. (For interpretation of the references to color in this figure legend, the reader is referred to the web version of this article.)

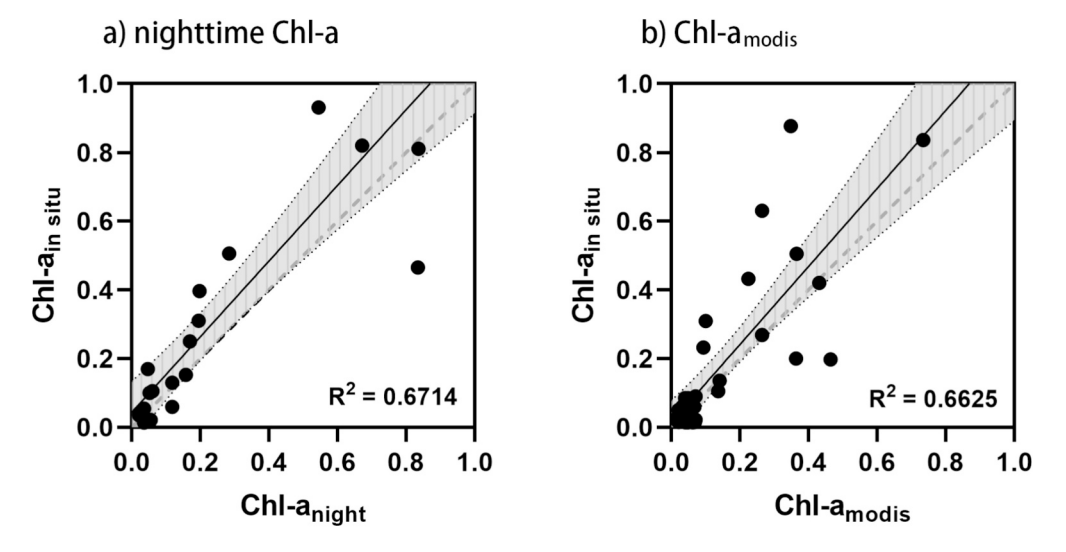


Fig. 14. a) is the fitting result of nocturnal Chl-a data and Chl-a $_{in\ situ}$. b) is the fitting result of Chl-a $_{modis}$ and Chl-a $_{in\ situ}$. The dashed lines are the 95 % confidence interval, the solid line is the fitting line, and the gray line is 1:1 line.

Table 3The metrics of algorithms assessment.

Metrics	Slope	Intercept	R ²	Bias	MAE
Nocturnal Chl-a and Chl-a _{in situ}	1.100	0.0439	0.6714	0.9796	1.8162
Chl-a _{modis} and Chl-a _{in situ}	1.135	0.0141	0.6625	1.2671	2.0059

This relationship may be associated with predator–prey dynamics within the plankton (Zhou et al., 2015). Studies have shown that the ratio of predator size to (ingested) prey size for distinct plankton grazer groups ranges, on average, over 1 to 2 orders of magnitude (Fernández-Álamo and Färber-Lorda, 2006; Wirtz, 2012; Zhou et al., 2015). This pattern may also encompass ecological flow within the plankton community and biological carbon pumps (Iversen, 2023; Legendre, 1999).

The nocturnal distribution of Chl-a can be derived from the diel difference in the 200 kHz acoustic data, which captures the nighttime patterns of larger suspended particles. Although the 200 kHz Sv data inherently include signals from vertically migrating fish and other plankton-feeding organisms (whose grazing activities contribute to phytoplankton consumption) and despite current limitations in accurately discriminating distinct biological signatures or eliminating their

C. Huang et al. Ecological Informatics 90 (2025) 103246

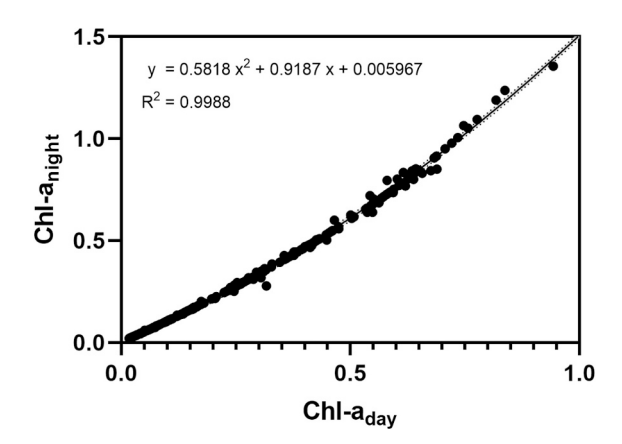


Fig. 15. The relationship between nocturnal Chl-a and diurnal Chl-a.

influences within acoustic data, the diel difference of 200 kHz Sv data, reflecting the overall organic particle dynamics in the water column, remains effective for reconstructing nocturnal Chl-a dynamics. Notably, the hyperbolic model may not capture specific phenomena, such as plankton anomalies from mesoscale eddies or algal blooms, because increased suspended particle concentrations reduce Sv data sensitivity, driving the model toward an extreme value (Fig. 10). This leads to model deviation when the Chl-a concentration is high, particularly when the C₃ component is dominant in the water. The same problems occur in the PSC algorithm, which is also a reason for model deviations (Brewin et al., 2010; Huan et al., 2022). Therefore, future research should further explore relevant ecological patterns and clarify the relationship between acoustic data and nocturnal Chl-a to develop a more accurate model.

In other words, this study establishes a methodological bridge between satellite-derived Chl-a and nocturnal Chl-a concentrations through acoustic Sv data analysis. The developed empirical relationships enable direct derivation of nocturnal Chl-a estimates from remote sensing data within the study area. And the derived nocturnal Chl-a products maintain spatiotemporal consistency with satellite observations, overcoming the inherent limitations of discrete field measurements, including low spatial coverage and scale mismatch. For broader applications, this framework provides a transferable methodology requiring region-specific validation through nocturnal Chl-a and coordinated acoustic sampling. Additionally, the stable relationship between the C₃ and 200 kHz frequency band data could extend the acoustic data of single-point station or transect surveys into large-scale applications by leveraging the characteristics of large-scale remote sensing surveys using the hyperbolic model. However, the accuracy of the large-scale acoustic data derived from the hyperbolic model still requires further verification, including the distribution of planktonic particles in the water column and their correlation with acoustic data; hence, we propose its feasibility.

4.3. The improvement of nocturnal Chl-a compared to Chl-a_{modis}

As a polar-orbiting satellite, MODIS-Aqua passes over the study area at approximately 13:30 local time. According to the diel variation of Chla in the Northwest Pacific Ocean, during this time, the concentration was relatively low, but gradually increased throughout the day (Pan et al., 2019). Therefore, using Chl-a $_{\rm modis}$ to represent the daily Chl-a level in the Northwest Pacific region may result in an overall underestimation of Chl-a concentration. This phenomenon may not be pronounced in low-latitude regions with low productivity; however, significant deviations may exist in areas with abundant nutrients and higher productivity, such as the Kuroshio–Oyashio Mixing Zone (Huang et al., 2022).

As shown in Table 3, the R² and slope show a slight improvement, and the systematic bias of the nocturnal Chl-a data is better than that of

Chl-a_{modis}. This is mainly because nocturnal Chl-a is obtained through relationships with Sv data and is not affected by variations in daylight intensity, which lead to deviations in Chl-amodis. Another factor contributing to the lower systematic bias of the nocturnal Chl-a was the manner in which the Sv-based algorithm accounted for the vertical distribution of particles in the water column. In contrast, the Chl-a_{modis} algorithm cannot accurately capture this vertical variability, particularly in complex oceanic environments with vigorous vertical mixing, such as upwelling regions (Blondeau-Patissier et al., 2014). This led to larger systematic errors in Chl-a_{modis}. Although the model may induce deviations (Discussion 4.2), nocturnal Chl-a data can reduce systematic biases compared with remote sensing Chl-a. For the satellite Chl-a product accuracy goal in the open ocean, an accuracy of approximately 35 % is generally considered acceptable for international missions (McClain, 2009). Therefore, compared to Chl- a_{modis} , the nocturnal Chl-a data can better reflect the distribution of phytoplankton in the Northwest Pacific Ocean, which can be further used to explore whether diel vertical migrations of zooplankton exhibit Chl-a concentration preferences (Garcia-Herrera et al., 2022; Ge et al., 2021). Specifically, since total Chl-a comprises size-fractionated phytoplankton components, and vertically migrating zooplankton (large body size) exhibit predatory preferences (Fernández-Álamo and Färber-Lorda, 2006; Wirtz, 2012; Zhou et al., 2015), regions with elevated nocturnal Chl-a concentrations reflect stronger influences from DVM activities. Compared to satellite-derived Chl-a (which typically represents surfacelayer or diurnally averaged concentrations), higher nighttime Chl-a levels further reflect the dominance of larger phytoplankton (C3 component) in water column and more pronounced diel migratory tendencies of zooplankton.

4.4. Ecological and fishery management insights from nocturnal Chl-a

Pan et al. and our study demonstrate that Chl-a has a diel variation with higher levels at night and lower levels during the day in the Northwest Pacific Ocean (Pan et al., 2019). This observed Chl-a diel variation not only reflects the adaptive regulation of phytoplankton to light-dark cycles but also provides a physiological basis for understanding their diurnal oscillation mechanisms. Smaller yet numerous nocturnal phytoplankton cells with high Chl-a contents are likely to be adequately prepared for photosynthesis and population growth during the day. Conversely, an increase in phytoplankton abundance during the daytime, along with light regulation, leads to a decrease in Chl-a content. These further confirm the results of Li et al., which show phytoplankton biomass and carbon content are lower at night and higher during the day, whereas cell abundance and size are smaller at night and larger during the day (Li et al., 2022). The decrease in nocturnal phytoplankton abundance and size was largely attributable to the upward movement of nocturnal zooplankton and fish during grazing (Ge et al., 2021). In contrast, the greater reduction in biomass and the higher Chl-a content of phytoplankton during the night highlight the richness of nutrients and biota in the corresponding marine region. In other words, nocturnal Chl-a data compensate for the lack of data on the diel variation of Chl-a and can effectively reveal the phenomenon of diurnalnocturnal oscillations in planktonic organisms, thus deepening our understanding of marine primary productivity and biological carbon cycling processes (Fogg, 1991; Legendre, 1999). By obtaining nocturnal Chl-a data, we can further assess the impact of diel vertical migration (DVM) on the increase in nocturnal zooplankton abundance in the upper ocean layers and their predation effects on the cycling of surface-layer materials (Fernández-Álamo and Färber-Lorda, 2006). Additionally, integrating nocturnal Chl-a data with other parameters, such as dissolved oxygen concentrations and nutrient levels, could provide a more comprehensive understanding of ocean ecosystem dynamics (Messié and Chavez, 2017).

In pelagic fisheries, a significant portion of commercial operations rely on nocturnal light-attraction fishing techniques to aggregate target species for capture. Therefore, some studies have combined acoustic and marine environmental remote-sensing data to explore fish habitats and stock distributions (Sánchez-Gendriz and Padovese, 2017; Xue et al., 2025; Zhu et al., 2024). Some studies have also combined ocean nighttime light remote sensing data and AIS vessel position data to monitor and manage ocean-going fishing vessels and further analysed the location of fishing grounds by integrating relevant environmental data (Tian et al., 2022). However, current marine environmental remote sensing data used in research are obtained mainly during the day. In contrast, nocturnal Chl-a data better reflect the distribution of nocturnal plankton. Nocturnal Chl-a data can better reflect the distribution of fish stocks and fishing operations for mid-surface economically important fish species that use plankton as forage organisms. Additionally, understanding the relationship between nocturnal Chl-a and fish migratory patterns can help predict the best time and location for fishing. Thus, compared to daytime data, nocturnal Chl-a data can assist managers and fishermen in more accurately identifying fishing grounds, enabling more precise planning and guidance of fishery activities based on the habits and life history characteristics of different economically important fish species. Furthermore, nocturnal Chl-a monitoring enables a more accurate delineation of fishery resource zones and ecological protection areas, providing a data-driven foundation for enhancing marine resource conservation and optimizing maritime supervision.

5. Conclusions

We aimed to determine the distribution of nocturnal Chl-a in the Northwestern Pacific Ocean by establishing a relationship between ocean color remote sensing data and Sv data collected using a multibeam fishery echosounder. The results demonstrate that the diel difference in 200 kHz Sv data can effectively reflect the distribution of larger suspended particles at night and correlates strongly with the C3 concentration derived from the PSC algorithm. Based on the relationship between C3 and Chl-a concentration, we successfully estimated the nocturnal Chl-a distribution using diurnal Chl-a data obtained from ocean color remote sensing. By analyzing the variations in diel Chl-a concentration, we achieved a better assessment of diel changes in phytoplankton and primary productivity in the ocean, providing insights into the diel migration of planktonic organisms, marine carbon cycles, and marine fisheries. However, the results obtained from this study apply to the Northwest Pacific Ocean, given the specific data collection and reprocessing process of the fishery echosounder Sv data. Further exploration is required to investigate the ecological patterns of plankton particles reflected in the acoustic data and Chl-a, to improve and validate the models. Additionally, efforts should be made to investigate seasonal and area differences.

CRediT authorship contribution statement

Chuanyang Huang: Writing – review & editing, Writing – original draft, Methodology, Investigation, Data curation, Conceptualization. Yang Liu: Writing – review & editing, Formal analysis, Conceptualization. Jianchao Li: Writing – review & editing, Formal analysis, Conceptualization. Hailing Wang: Methodology, Data curation. Yanping Luo: Methodology, Data curation. Honghai Zhang: Data curation. Zhaohui Chen: Data curation.

Declaration of competing interest

The authors declare that they have no known competing financial interests or personal relationships that could have appeared to influence the work reported in this paper.

Acknowledged

This work was supported by National Key Research and

Development Program of China (2023YFD2401305), and the National Natural Science Foundation of China (42225601 and 42176006). The survey and data used in this paper was supported by the Laoshan Laboratory (grant number LSKJ202201701). The satellite chlorophyll data of MODIS-aqua was provided by NASA (National Aeronautics and Space Administration).

Data availability

Ocean color remote sensing Chl-a data in this study are available from https://oceancolor.gsfc.nasa.gov/, the fishery echosounder acoustic data and surface Chl-a data are available on Figshare (https://figshare.com/s/57946e9f209ce5689361).

References

- Agarwal, S., Rocchini, D., Marathe, A., Nagendra, H., 2016. Exploring the relationship between remotely-sensed spectral variables and attributes of tropical Forest vegetation under the influence of local Forest institutions. ISPRS Int. J. Geo Inf. 5, 117. https://doi.org/10.3390/ijgi5070117.
- Ariza, A., Garijo, J.C., Landeira, J.M., Bordes, F., Hernández-León, S., 2015. Migrant biomass and respiratory carbon flux by zooplankton and micronekton in the subtropical Northeast Atlantic Ocean (Canary Islands). Prog. Oceanogr. 134, 330–342. https://doi.org/10.1016/j.pocean.2015.03.003.
- Béhagle, N., Cotté, C., Ryan, T.E., Gauthier, O., Roudaut, G., Brehmer, P., Josse, E., Cherel, Y., 2016. Acoustic micronektonic distribution is structured by macroscale oceanographic processes across 20–50°S latitudes in the South-Western Indian Ocean. Deep-Sea Res. I Oceanogr. Res. Pap. 110, 20–32. https://doi.org/10.1016/j. dsr.2015.12.007.
- Behrenfeld, M.J., Gaube, P., Della Penna, A., O'Malley, R.T., Burt, W.J., Hu, Y., Bontempi, P.S., Steinberg, D.K., Boss, E.S., Siegel, D.A., Hostetler, C.A., Tortell, P.D., Doney, S.C., 2019. Global satellite-observed daily vertical migrations of ocean animals. Nature 576, 257–261. https://doi.org/10.1038/s41586-019-1796-9.
- Blondeau-Patissier, D., Gower, J.F.R., Dekker, A.G., Phinn, S.R., Brando, V.E., 2014. A review of ocean color remote sensing methods and statistical techniques for the detection, mapping and analysis of phytoplankton blooms in coastal and open oceans. Prog. Oceanogr. 123, 123–144. https://doi.org/10.1016/j. pocean.2013.12.008.
- Boyce, D.G., Lewis, M.R., Worm, B., 2010. Global phytoplankton decline over the past century. Nature 466, 591–596. https://doi.org/10.1038/nature09268.
- Brewin, R.J.W., Sathyendranath, S., Hirata, T., Lavender, S.J., Barciela, R.M., Hardman-Mountford, N.J., 2010. A three-component model of phytoplankton size class for the Atlantic Ocean. Ecol. Model. 221, 1472–1483. https://doi.org/10.1016/j.ecol.padel.2010.2014.
- Brewin, R.J.W., Hardman-Mountford, N.J., Lavender, S.J., Raitsos, D.E., Hirata, T., Uitz, J., Devred, E., Bricaud, A., Ciotti, A., Gentili, B., 2011. An intercomparison of bio-optical techniques for detecting dominant phytoplankton size class from satellite remote sensing. Remote Sens. Environ. 115, 325–339. https://doi.org/10.1016/j. rse.2010.09.004.
- Carlsen, A.A., Casini, M., Masnadi, F., Olsson, O., Hejdström, A., Hentati-Sundberg, J., 2024. Autonomous data sampling for high-resolution spatiotemporal fish biomass estimates. Ecol. Inform. 84, 102852. https://doi.org/10.1016/j.ecoinf.2024.102852.
- Chai, F., Wang, Y., Xing, X., Yan, Y., Xue, H., Wells, M., Boss, E., 2021. A limited effect of sub-tropical typhoons on phytoplankton dynamics. Biogeosciences 18, 849–859. https://doi.org/10.5194/bg-18-849-2021.
- Chiba, S., Di Lorenzo, E., Davis, A., Keister, J.E., Taguchi, B., Sasai, Y., Sugisaki, H., 2013. Large-scale climate control of zooplankton transport and biogeography in the Kuroshio-Oyashio extension region. Geophys. Res. Lett. 40, 5182–5187. https://doi. org/10.1002/grl.50999.
- Doblin, M.A., Petrou, K.L., Shelly, K., Westwood, K., Van Den Enden, R., Wright, S., Griffiths, B., Ralph, P.J., 2011. Diel variation of chlorophyll-a fluorescence, phytoplankton pigments and productivity in the sub-Antarctic and polar front zones south of Tasmania. Australia. Deep Sea Res. Part II 58, 2189–2199. https://doi.org/10.1016/j.dsr2.2011.05.021.
- Dutkiewicz, S., Hickman, A.E., Jahn, O., Henson, S., Beaulieu, C., Monier, E., 2019.
 Ocean colour signature of climate change. Nat. Commun. 10, 578. https://doi.org/10.1038/s41467-019-08457-x.
- Everett, J.D., Baird, M.E., Buchanan, P., Bulman, C., Davies, C., Downie, R., Griffiths, C., Heneghan, R., Kloser, R.J., Laiolo, L., Lara-Lopez, A., Lozano-Montes, H., Matear, R. J., McEnnulty, F., Robson, B., Rochester, W., Skerratt, J., Smith, J.A., Strzelecki, J., Suthers, I.M., Swadling, K.M., Van Ruth, P., Richardson, A.J., 2017. Modeling what we sample and sampling what we model: challenges for zooplankton model assessment. Front. Mar. Sci. 4. https://doi.org/10.3389/fmars.2017.00077.
- Falkowski, P.G., Katz, M.E., Knoll, A.H., Quigg, A., Raven, J.A., Schofield, O., Taylor, F.J. R., 2004. The evolution of modern eukaryotic phytoplankton. Science 305, 354–360. https://doi.org/10.1126/science.1095964.
- Fan, W., Wu, Y., Cui, X., 2009. The study on fishing ground of neon flying squid, Ommastrephes bartrami, and ocean environment based on remote sensing data in the Northwest Pacific Ocean. Chin. J. Oceanol. Limnol. 27, 408–414. https://doi. org/10.1007/s00343-009-9107-1.

- FAO, 2019. FAO yearbook. Fishery and Aquaculture Statistics 2017/FAO annuaire. Statistiques des pêches et de l'aquaculture 2017/FAO anuario. Estadísticas de pesca y acuicultura. 2017.
- Fernández-Álamo, M.A., Färber-Lorda, J., 2006. Zooplankton and the oceanography of the eastern tropical Pacific: a review. Prog. Oceanogr. 69, 318–359. https://doi.org/ 10.1016/j.pocean.2006.03.003.
- Field, C.B., Behrenfeld, M.J., Randerson, J.T., Falkowski, P., 1998. Primary production of the biosphere: integrating terrestrial and oceanic components. Science 281, 237–240. https://doi.org/10.1126/science.281.5374.237.
- Fogg, G.E., 1991. The phytoplanktonic ways of life. New Phytol. 118, 191–232. https://doi.org/10.1111/j.1469-8137.1991.tb00974.x.
- Foote, K.G., Knudsen, H.P., Vestnes, G., 1987. Calibration of Acoustic Instruments for Fish Density Estimation: A Practical Guide. https://doi.org/10.17895/ICES. PUB.8265.
- Friedland, K.D., Stock, C., Drinkwater, K.F., Link, J.S., Leaf, R.T., Shank, B.V., Rose, J.M., Pilskaln, C.H., Fogarty, M.J., 2012. Pathways between primary production and fisheries yields of large marine ecosystems. PLoS One 7, e28945. https://doi.org/ 10.1371/journal.pone.0028945.
- Fujioka, E., Soldevilla, M.S., Read, A.J., Halpin, P.N., 2014. Integration of passive acoustic monitoring data into OBIS-SEAMAP, a global biogeographic database, to advance spatially-explicit ecological assessments. Ecol. Inform. 21, 59–73. https:// doi.org/10.1016/j.ecoinf.2013.12.004.
- Garcia-Herrera, N., Cornils, A., Laudien, J., Niehoff, B., Höfer, J., Försterra, G., González, H.E., Richter, C., 2022. Seasonal and diel variations in the vertical distribution, composition, abundance and biomass of zooplankton in a deep Chilean Patagonian Fjord. PeerJ 10, e12823. https://doi.org/10.7717/peerj.12823.
- Ge, R., Chen, H., Zhuang, Y., Liu, G., 2021. Active carbon flux of Mesozooplankton in South China Sea and Western Philippine Sea. Front. Mar. Sci. 8, 697743. https://doi. org/10.3389/fmars.2021.697743.
- Guan, Z., Ge, R., Li, Y., Zou, L., Yang, S., 2023. Diel variation of phytoplankton communities in the northern South China Sea under the effect of internal solitary waves and its response to environmental factors. Water 15, 2422. https://doi.org/ 10.3390/w15132422.
- Hays, G., Richardson, A., Robinson, C., 2005. Climate change and marine plankton. Trends Ecol. Evol. 20, 337–344. https://doi.org/10.1016/j.tree.2005.03.004.
- Hilligsøe, K.M., Richardson, K., Bendtsen, J., Sørensen, L.-L., Nielsen, T.G., Lyngsgaard, M.M., 2011. Linking phytoplankton community size composition with temperature, plankton food web structure and sea–air CO2 flux. Deep-Sea Res. I Oceanogr. Res. Pap. 58, 826–838. https://doi.org/10.1016/j.dsr.2011.06.004.
- Holliday, D., 1995. Bioacoustical oceanography at high frequencies. ICES J. Mar. Sci. 52, 279–296. https://doi.org/10.1016/1054-3139(95)80044-1.
- Huan, Y., Sun, D., Wang, S., Zhang, H., Li, Z., He, Y., 2022. Phytoplankton size classes in the Global Ocean at different bathymetric depths. IEEE Trans. Geosci. Remote Sens. 60, 1–11. https://doi.org/10.1109/TGRS.2022.3153477.
- Huang, C., Liu, Y., Luo, Y., Wang, Y., Liu, X., Zhang, Y., Zhuang, Y., Tian, Y., 2022. Improvement and assessment of ocean color algorithms in the Northwest Pacific fishing ground using Himawari-8, MODIS-aqua, and VIIRS-SNPP. Remote Sens. 14, 3610. https://doi.org/10.3390/rs14153610.
- Iversen, M.H., 2023. Carbon export in the ocean: a biologist's perspective. Annu. Rev. Mar. Sci. 15, 357–381. https://doi.org/10.1146/annurev-marine-032122-035153.
- Kande, Y., Diogoul, N., Brehmer, P., Dabo-Niang, S., Ngom, P., Perrot, Y., 2024. Demonstrating the relevance of spatial-functional statistical analysis in marine ecological studies: the case of environmental variations in micronektonic layers. Ecol. Inform. 81, 102547. https://doi.org/10.1016/j.ecoinf.2024.102547.
- Lavery, A.C., Wiebe, P.H., Stanton, T.K., Lawson, G.L., Benfield, M.C., Copley, N., 2007. Determining dominant scatterers of sound in mixed zooplankton populations. J. Acoust. Soc. Am. 122, 3304–3326. https://doi.org/10.1121/1.2793613.
- Legendre, L., 1999. Chlorophyll a to estimate the particulate organic carbon available as food to large zooplankton in the euphotic zone of oceans. J. Plankton Res. 21, 2067–2083. https://doi.org/10.1093/plankt/21.11.2067.
- Li, C., Chiang, K., Laws, E.A., Liu, X., Chen, J., Huang, Y., Chen, B., Tsai, A., Huang, B., 2022. Quasi-antiphase diel patterns of abundance and cell size/biomass of picophytoplankton in the Oligotrophic Ocean. Geophys. Res. Lett. 49, e2022GL097753. https://doi.org/10.1029/2022GL097753.
- McClain, C.R., 2009. A decade of Satellite Ocean color observations. Annu. Rev. Mar. Sci. 1, 19–42. https://doi.org/10.1146/annurev.marine.010908.163650.
- McManus, M.A., Woodson, C.B., 2012. Plankton distribution and ocean dispersal. J. Exp. Biol. 215, 1008–1016. https://doi.org/10.1242/jeb.059014.
- Messié, M., Chavez, F.P., 2017. Nutrient supply, surface currents, and plankton dynamics predict zooplankton hotspots in coastal upwelling systems. Geophys. Res. Lett. 44, 8979–8986. https://doi.org/10.1002/2017GL074322.
- Neveux, J., Dupouy, C., Blanchot, J., Le Bouteiller, A., Landry, M.R., Brown, S.L., 2003. Diel dynamics of chlorophylls in high-nutrient, low-chlorophyll waters of the equatorial Pacific (180°): interactions of growth, grazing, physiological responses, and mixing. J. Geophys. Res. Oceans 108, 2000JC000747. https://doi.org/10.1029/ 2000JC000747.
- Nie, L., Li, J., Liu, Y., Sun, P., Ye, Z., Zhang, H., Zhu, L., Ma, S., Zhang, W., Tian, Y., 2023. Spatial and temporal characteristics of winter diel vertical migration of zooplankton and nekton in the East China shelf seas based on multi-frequency echosounder.

- J. Geophys. Res. Oceans 128, e2023JC020426. https://doi.org/10.1029/2023JC020426.
- Pan, X., Wong, G.T.F., Ho, T.-Y., Tai, J.-H., 2019. Diel variability of vertical distributions of chlorophyll a at the SEATS and ALOHA stations: implications on remote sensing interpretations. Int. J. Remote Sens. 40, 2916–2935. https://doi.org/10.1080/ 01431161.2018.1538583.
- Sánchez-Gendriz, I., Padovese, L.R., 2017. Temporal and spectral patterns of fish choruses in two protected areas in southern Atlantic. Ecol. Inform. 38, 31–38. https://doi.org/10.1016/j.ecoinf.2017.01.003.
- Schwartz-Belkin, I., Portman, M.E., 2023. A review of geospatial technologies for improving marine spatial planning: challenges and opportunities. Ocean Coast. Manag. 231, 106280. https://doi.org/10.1016/j.ocecoaman.2022.106280.
- Seegers, B.N., Stumpf, R.P., Schaeffer, B.A., Loftin, K.A., Werdell, P.J., 2018.
 Performance metrics for the assessment of satellite data products: an ocean color case study. Opt. Express 26, 7404. https://doi.org/10.1364/OE.26.007404.
- Stanton, T., 2000. Review and recommendations for the modelling of acoustic scattering by fluid-like elongated zooplankton: euphausiids and copepods. ICES J. Mar. Sci. 57, 793–807. https://doi.org/10.1006/jmsc.1999.0517.
- Swartzman, G., Brodeur, R., Napp, J., Walsh, D., Hewitt, R., Demer, D., Hunt, G., Logerwell, E., 1999. Relating Spatial Distributions of Acoustically Determined Patches of Fish and Plankton: Data Viewing, Image Analysis, and Spatial Proximity. https://doi.org/10.1139/f99-206.
- Tian, H., Liu, Y., Tian, Y., Alabia, I.D., Qin, Y., Sun, H., Li, J., Ma, S., Saitoh, S.-I., 2022. A comprehensive monitoring and assessment system for multiple fisheries resources in the Northwest Pacific based on satellite remote sensing technology. Front. Mar. Sci. 9, 808282. https://doi.org/10.3389/fmars.2022.808282.
- Tokarev, Yu.N., Williams, R., Piontkovski, S.A., 1998. Small-scale plankton patchiness in the Black Sea euphotic layer. Hydrobiologia 375 (376), 363–367. https://doi.org/10.1023/A:1017003410651.
- Turner, K.J., Mouw, C.B., Hyde, K.J.W., Morse, R., Ciochetto, A.B., 2021. Optimization and assessment of phytoplankton size class algorithms for ocean color data on the northeast U.S. continental shelf. Remote Sens. Environ. 267, 112729. https://doi. org/10.1016/j.rse.2021.112729.
- Uitz, J., Claustre, H., Morel, A., Hooker, S.B., 2006. Vertical distribution of phytoplankton communities in open ocean: an assessment based on surface chlorophyll. J. Geophys. Res. 111, C08005. https://doi.org/10.1029/ 2005.IC003207.
- Ventero, A., Iglesias, M., Miquel, J., 2020. From coast to slope: zooplankton communities shift in the northern Alboran Sea. Estuar. Coast. Shelf Sci. 242, 106854. https://doi. org/10.1016/j.ecss.2020.106854.
- Wang, Y., Tang, R., Yu, Y., Ji, F., 2021. Variability in the sea surface temperature gradient and its impacts on chlorophyll-a concentration in the Kuroshio extension. Remote Sens. 13, 888. https://doi.org/10.3390/rs13050888.
- Wei, Y., Chen, X., Liu, Y., Wang, Y., Qu, K., Sun, J., Cui, Z., 2023. Key determinants controlling the seasonal variation of coastal zooplankton communities: a case study along the Yellow Sea. Mar. Pollut. Bull. 193, 115175. https://doi.org/10.1016/j.marpolbul.2023.115175.
- Wirtz, K., 2012. Who is eating whom? Morphology and feeding type determine the size relation between planktonic predators and their ideal prey. Mar. Ecol. Prog. Ser. 445, 1–12. https://doi.org/10.3354/meps09502.
- Xi, H., Losa, S.N., Mangin, A., Soppa, M.A., Garnesson, P., Demaria, J., Liu, Y., d'Andon, O.H.F., Bracher, A., 2020. Global retrieval of phytoplankton functional types based on empirical orthogonal functions using CMEMS GlobColour merged products and further extension to OLCI data. Remote Sens. Environ. 240, 111704. https://doi.org/10.1016/j.rse.2020.111704.
- Xue, M., Tong, J., Tian, S., Wang, X., 2021. Broadband characteristics of Zooplankton sound scattering layer in the Kuroshio–Oyashio confluence region of the Northwest Pacific Ocean in summer of 2019. J. Mar. Sci. Eng. 9, 938. https://doi.org/10.3390/ jmse9090938.
- Xue, M., Tong, J., Ma, W., Zhu, Z., Wang, W., Lyu, S., Chen, X., 2025. Reimagining habitat suitability modeling for Pacific saury (*Cololabis saira*) in the Northwest Pacific Ocean through acoustic data analysis from fishing vessels. Ecol. Inform. 85, 102971. https://doi.org/10.1016/j.ecoinf.2024.102971.
- Yatsu, A., Chiba, S., Yamanaka, Y., Ito, S., Shimizu, Y., Kaeriyama, M., Watanabe, Y., 2013. Climate forcing and the Kuroshio/Oyashio ecosystem. ICES J. Mar. Sci. 70, 922–933. https://doi.org/10.1093/icesjms/fst084.
- Zang, Y., Chen, H., Zhuang, Y., Ge, R., Wang, W., Liu, G., 2023. Latitudinal transition of epipelagic mesozooplankton in the northwestern Pacific in winter. Mar. Environ. Res. 186, 105915. https://doi.org/10.1016/j.marenvres.2023.105915.
- Zhou, L., Tan, Y., Huang, L., Hu, Z., Ke, Z., 2015. Seasonal and size-dependent variations in the phytoplankton growth and microzooplankton grazing in the southern South China Sea under the influence of the east Asian monsoon. Biogeosciences 12, 6809–6822. https://doi.org/10.5194/bg-12-6809-2015.
- Zhou, J., Zhou, G., Liu, H., Li, Z., Cheng, X., 2021. Mesoscale Eddy-Induced Ocean dynamic and thermodynamic anomalies in the North Pacific. Front. Mar. Sci. 8, 756918. https://doi.org/10.3389/fmars.2021.756918.
- Zhu, Z., Tong, J., Xue, M., Sarr, O., Gao, T., 2024. Assessing the influence of abiotic factors on small pelagic fish distribution across diverse water layers in the Northwest Pacific Ocean through acoustic methods. Ecol. Indic. 158, 111563. https://doi.org/ 10.1016/j.ecolind.2024.111563.